

APRIL 06 2023

Guided wave propagation and skew effects in anisotropic carbon fiber reinforced laminates **FREE**

Flora Hervin ; Paul Fromme



J Acoust Soc Am 153, 2049 (2023)

<https://doi.org/10.1121/10.0017784>

Selectable Content List

- Low frequency ambient noise dynamics and trends in the Indian Ocean, Cape Leeuwin, Australia
- Age-related reduction of amplitude modulation frequency selectivity
- Intra- and inter-speaker variation in eight Russian fricatives
- Estimating cochlear impulse responses using frequency sweeps
- A characteristic nonlinear distortion length for broadband Gaussian noise



View
Online



Export
Citation

CrossMark

Related Content

Behavior of laminated composite skew plates under different temperature variations

AIP Conference Proceedings (July 2019)

3D guided wave motion analysis on laminated composites

AIP Conference Proceedings (February 2014)

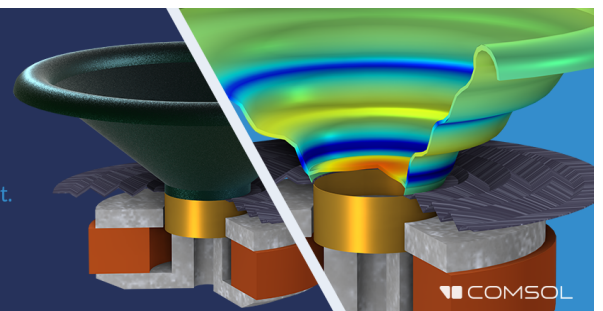
Effect of skew angle on second harmonic guided wave measurement in composite plates

AIP Conference Proceedings (February 2017)

Take the Lead in Acoustics



The ability to account for coupled physics phenomena lets you predict, optimize, and virtually test a design under real-world conditions – even before a first prototype is built.

» Learn more about **COMSOL Multiphysics®**



COMSOL

Guided wave propagation and skew effects in anisotropic carbon fiber reinforced laminates

Flora Hervin^{a)}  and Paul Fromme 

Department of Mechanical Engineering, University College London (UCL), London, WC1E 7JE, United Kingdom

ABSTRACT:

Guided ultrasonic waves provide a promising structural health monitoring (SHM) solution for composite structures as they are able to propagate relatively long distances with low attenuation. However, the material anisotropy results in directionally dependent phase and group velocities, in addition to energy focusing, wave skewing, and beam spreading phenomena. These effects could lead to inaccurate damage localization if not accounted for. In this contribution, the guided wave propagation behavior (A_0 mode) for a highly anisotropic, unidirectional carbon fiber reinforced polymer laminate is systematically investigated through both finite element analysis and non-contact laser measurements and compared to theoretical predictions. The directional dependency of phase and group velocity measured for a point and line source shows good agreement with theoretical predictions, once a correction for wave skew effects is applied. Wave skew angles were evaluated from the experimental and numerical wave propagation in multiple directions and matched theoretical predictions based on the phase slowness curve. Significant guided wave beam spreading from a line source was observed and quantified from both experiments and simulations and compared with theoretical predictions using the anisotropy factor. The impact of anisotropic guided wave propagation behavior on SHM is discussed. © 2023 Acoustical Society of America. <https://doi.org/10.1121/10.0017784>

(Received 23 October 2022; revised 3 February 2023; accepted 19 March 2023; published online 6 April 2023)

[Editor: Li Cheng]

Pages: 2049–2060

I. INTRODUCTION

Carbon fiber reinforced polymer (CFRP) laminates are widely used for aerospace components due to their good strength to weight ratio. They consist of highly anisotropic fiber-matrix ply layers with high in-plane stiffness along the fiber directions.¹ However, poor interlaminar strength means that composite laminates are prone to barely visible impact damage (BVID) caused by low velocity impacts.² Matrix cracking, fiber breakage, and delamination can occur, reducing laminate stiffness and potentially leading to catastrophic failure of the component.³ Guided ultrasonic waves provide a promising structural health monitoring (SHM) solution for rapid inspection and monitoring of composites as they can propagate over long distances. Unlike isotropic structures, however, wave propagation in composites results in directional dependency of velocity, wave skewing, and beam spreading behavior, caused by the material anisotropy.⁴ These anisotropic effects need to be considered as they could lead to errors in locating damage, and worst case to regions of the laminate where waves do not penetrate.⁵ Therefore, understanding guided wave propagation in the presence of anisotropy is required to develop accurate SHM systems for composite structures.

Guided ultrasonic waves can be employed for the rapid scanning of large areas.⁶ Often, the fundamental symmetric S_0 and antisymmetric A_0 modes at low frequency are selected for SHM in composites, as they are below the cutoff frequencies of higher order modes, simplifying signal

processing⁷ in addition to minimizing attenuation.⁸ The S_0 mode has been used in numerous studies.^{9–11} At low frequencies, the S_0 mode is less dispersive and has a higher propagation velocity than the A_0 mode, and therefore is easy to distinguish as the first arrival pulse. However, no S_0 mode reflection occurs at interfaces with zero shear strain, and so damage located at these depths would not be detected.¹² The A_0 mode is sensitive to damage at all depths and has a shorter wavelength than the S_0 mode at the same frequency, improving sensitivity to smaller defects.¹² Guided wave propagation can be described by the phase, group, and energy velocities. In isotropic materials, the phase, group, and energy velocity directions are the same, but this is not the case in highly attenuating and anisotropic materials.¹³ While composites do experience wave attenuation due to scattering at the fibers and damping from the matrix, the attenuation is low enough that the approximation of group velocity as equal to energy velocity still holds in general.⁵

Guided wave velocities in composite laminates are directionally dependent, with higher velocities in the high stiffness (fiber) directions. As guided wave mode velocities are also frequency dependent, this leads to dispersion curves being three-dimensional (3D). Damage detection and localization are therefore more complex than for an isotropic structure. In unidirectional CFRP, the A_0 mode has lower directional variation than the S_0 mode, although still significant enough to impact damage detection.¹⁴ In anisotropic materials wave energy tends to be focused away from the wave launching direction towards the fiber directions, i.e., phase and group directions are no longer equal.¹⁵ The energy of the wave packet is

^{a)}Electronic mail: flora.hervin.19@ucl.ac.uk

steered along the group direction, but the wavefronts remain perpendicular to the wave launching (phase) direction.¹⁶ The extent of the wave steering can be defined using the wave skew angle, which is the angular difference between the group and phase directions. The group direction is defined as the normal to the phase slowness curve, which is in turn defined as the inverse of the phase velocity.¹⁷ Accurate knowledge of the phase slowness curve is essential for the prediction of anisotropic effects. The extent of directional dependence of velocity and wave skewing is layup dependent. Severe skew angles up to 40° are possible in composites.¹⁸ In addition to wave skewing, beam spreading can also occur. The ultrasonic beam widens as it propagates, with the degree of widening being directionally dependent. Increased widening is observed if the beam is launched away from the fiber directions (directions with lower stiffness) and is more pronounced for the S₀ mode than the A₀ mode.¹⁹

Anisotropic effects can impact a variety of guided wave SHM techniques. For phased array imaging, delay-and-sum beamforming was modified with phase delays calculated to account for the skew angle and directionally dependent wave velocity.^{20,21} Wave skew effects can sometimes be avoided by using wave launching directions that exploit material symmetry or quasi-isotropic mode points.²² Quasi-isotropic mode points are particular modes and frequencies with almost circular slowness curves, and therefore minimal wave skew; however, such mode points may not exist in every composite structure.²³ Anisotropy has been shown to strongly influence amplitudes of scattered waves around a delamination in CFRP,¹⁴ with focusing along the fiber orientation of the outer layers of the composite laminate,²³ which could impact the accuracy of sparse array imaging.²⁴

The theoretical basis for wave propagation in anisotropic materials has been well established. Ogilvy²⁵ introduced the divergence D , a dimensionless quantity describing the rate of widening of an acoustic beam due to anisotropy, defined as the change in group direction θ_{group} , with respect to phase direction θ_{phase} ,

$$D = \left| \frac{d\theta_{group}}{d\theta_{phase}} \right|. \quad (1)$$

An isotropic material would have no additional beam divergence due to anisotropy ($D = 1$, phase and group direction aligned), while $D > 1$ indicates an increased rate of beam widening and $D < 1$ a reduced rate of beam widening due to anisotropy. Newberry and Thompson²⁶ represented a bulk ultrasonic beam propagating in an anisotropic medium using a series of Gauss-Hermite solutions in the far field. They introduced the anisotropy factor, which was shown to be related to the divergence as

$$A = (\cos(\theta_{skew}))^{-2} \cdot D, \quad (2)$$

where θ_{skew} is the wave skew angle. Karmazin developed an asymptotic solution in the far field for Lamb waves excited in composite plates. Wave energy focusing in anisotropic

materials has been shown to be analogue to the phonon focusing effect that occurs in crystalline structures²⁷ and the “walk off” angle terminology in the field of crystal acoustics is equivalent to the wave skew angle.^{28,29} Chapuis *et al.*³⁰ derived an analytical expression of the Green’s function for Lamb waves in the far field and showed that the anisotropy of the propagation direction induced strong focusing of Lamb modes in CFRP plates. They found that focusing directions correspond to the minima of the slowness curves. Potel *et al.*³¹ used plane wave decomposition of the incident wave beam to determine the wave skew angle. Experimental and numerical results illustrated the strong deviation towards fibers in a unidirectional plate predicted by the theoretical results. Chronopoulos³² expressed the wave skew angle as a function of the material properties of an anisotropic structure and proposed an efficient Finite Element Analysis (FEA) method that matched the theoretical predictions. Biot’s energy approach was extended to derive the Lamb wave group velocity and subsequently skew angle in a composite plate³³ and showed good agreement with FEA predictions.³⁴

Relatively few studies have considered anisotropic wave propagation effects experimentally. Several studies have considered the directionality of the group/energy velocity in anisotropic materials,^{4,16,35–37} but relatively few have experimentally measured phase velocities in multiple wave propagation directions.³⁸ Lamb wave propagation in monocrystalline silicon wafers was investigated experimentally and numerically. Measured wave skew angles were well matched for the A₀ mode but a systematic offset was observed for the S₀ mode.¹⁹ Beam spreading was also shown to increase as the orientation of the incident guided wave beam moved away from the high stiffness directions, but comparison to theoretical predictions was not investigated. Putkis *et al.*⁴ measured strong directional dependency of the energy velocity for the S₀, SH₀, and A₀ modes in a unidirectional CFRP plate. Chapuis *et al.*³⁹ demonstrated energy focusing along the fiber directions of the A₀ and S₀ modes generated by a lead zirconate titanate (PZT) disk in cross-ply CFRP through wavefield measurements and demonstrated that the energy focusing effect can be described by the Maris factor. Salas and Cesnik⁴⁰ used a ring-shaped transducer with multiple elements to launch waves in different directions and used wavefield imaging to qualitatively demonstrate the wave steering behavior in unidirectional, cross-ply, and quasi-isotropic laminates, but skew angles were not quantified or compared to theoretical predictions. Potel *et al.*³¹ measured the wave skew angle of the S₀ mode in a single wave propagation direction, showing good agreement with predicted angles. Lowe *et al.*⁵ used a line source consisting of multiple PZT discs to launch waves at 20° to the fiber direction in unidirectional CFRP and measured a steering angle consistent with theoretical predictions.

This contribution aims to systematically investigate wave skew angles and beam spreading in a highly anisotropic plate, comparing FE modelling and experimental measurements with theoretical predictions. Phase and group velocities of the A₀ guided wave mode in a unidirectional

TABLE I. Orthotropic stiffness constants and density of the unidirectional CFRP specimen. All values in GPa unless otherwise stated. Obtained at 2 MHz at the University of Bordeaux, France (Ref. 35).

C11	12.56
C12	6.87
C13	6.47
C22	13.15
C23	5.60
C33	109.90
C44	4.70
C55	4.00
C66	2.27
ρ (kgm ⁻³)	1550

CFRP plate were measured for multiple wave propagation directions. Full 3D FEA simulations were developed to model wave propagation from both point and line sources. Non-contact laser measurements were performed to validate simulations. The wave skew angles from a line source were investigated numerically and experimentally and compared to theoretical predictions. The beam spreading phenomena is quantified and compared to theoretical predictions. The paper is structured as follows: Sec. II describes the finite element simulations used to model wave propagation, followed by details of the experimental measurements in Sec. III. Section IV provides a comparison between experiment, FEA, and theoretical predictions for velocity variation with propagation direction, wave skewing, and beam spreading. Conclusions are drawn in Sec. V.

II. FINITE ELEMENT MODELING

Full 3D FEA simulations of a unidirectional CFRP plate section with dimensions 600 mm × 400 mm × 3.6 mm were carried out in ABAQUS/Explicit. A model input file, specifying parameters and geometry, was generated in MATLAB before being imported into ABAQUS 2018 for analysis. The plate was modelled as an anisotropic, homogenized structure with material properties given in Table I. Eight node solid brick elements (C3D8R) were selected for the model with

an element size of 0.5 mm × 0.5 mm × 0.45 mm to obtain eight elements through the plate thickness and at least 30 elements per wavelength in the in-plane direction. The time increment was set to 5 ns and the simulation time was set to 150 μs, fulfilling the usual stability criteria.⁴¹ Stiffness proportional Rayleigh damping was included to model attenuation in the plate. The damping coefficient was set to $\beta = 70$ ns. Point source excitation of the A₀ mode was implemented by applying an out-of-plane force to a single node. The narrowband excitation pulse was a 75 kHz, 5-cycle sine wave modified by a Hanning window. A line excitation was generated by applying simultaneous out-of-plane forces along a line of nodes, 40 mm in length.

For the phase and group velocity characterization, history outputs for the out-of-plane displacements were requested along a 100 mm line of monitoring points, originating 100 mm from the excitation with a step size of 1 mm, as shown in Fig. 1(a). Additionally, for the 40 mm line excitation, a 100 mm line of measurement points directed along the wave skew angle was defined. In order to model wave propagation in different incident wave directions, the orientation of the material properties was rotated while keeping the model geometry and monitoring locations the same. Material properties were rotated in 5° steps between 0° and 90°. A separate simulation was performed in each direction for each excitation type. Wave skew and beam widening effects were investigated for the 40 mm line excitation by recording out of plane displacements along five lines of measurement points (parallel to line excitation), spanning the full width of the plate. The lines were located 100, 125, 150, 175, and 200 mm from the excitation location as shown in Fig. 1(b). A separate simulation was again performed for each incident wave direction.

Theoretical phase and group velocity dispersion curves were obtained using Disperse software⁴² for a 3.6 mm thick unidirectional CFRP panel with the material properties given in Table I. A separate set of dispersion curves was calculated for wave propagation directions between 0° and 90° in 5° increments to obtain theoretical values for each angle relative to the fiber orientation. The theoretical phase

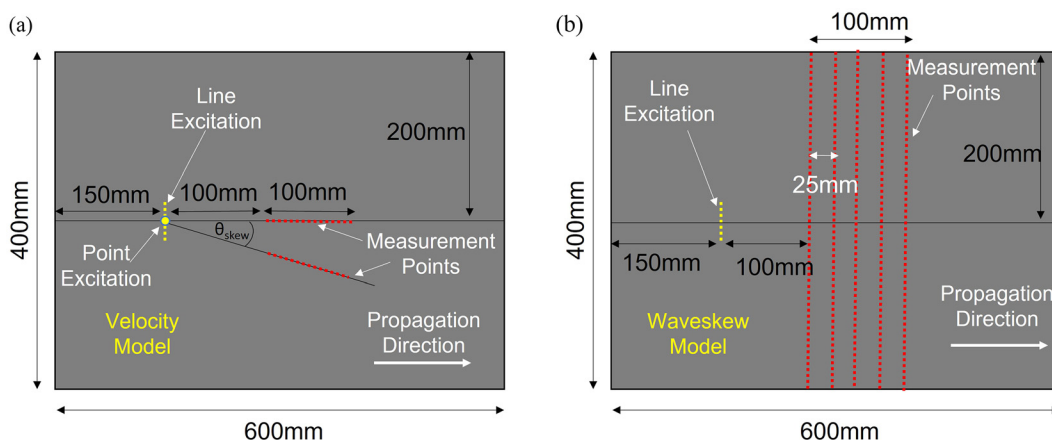


FIG. 1. (Color online) Geometry of finite element (FE) model. Schematic shows excitation and measurement locations for (a) velocity simulations; (b) wave skew simulations.

slowness curve was calculated for the A_0 mode at 75 kHz, as shown in Fig. 2(a). Theoretical wave skew values for each incident wave direction were then calculated from the slowness curve by calculating the difference between the group and phase directions. The group direction was calculated by taking the normal of the tangent to the slowness curve at a particular phase direction, as shown schematically in the diagram in Fig. 2(a). The skew angle can then be calculated from the difference between the phase and group directions. The theoretical values for the wave skew angle are shown in Fig. 2(b). As expected, zero skew angle is observed in the principal (0° and 90°) directions. The highest skew angle of 25° is predicted in the 45° direction.

III. EXPERIMENTAL MEASUREMENTS

Guided wave measurements were performed on a 24-ply unidirectional CFRP panel with nominal dimensions $1.14\text{ m} \times 0.94\text{ m}$. The plate thickness was 3.6 mm, giving a ply thickness of 0.15 mm. The previously measured material properties are given in Table I.³⁵

A piezoceramic transducer (5 mm diameter, 2 mm thickness) with brass backing mass (5 mm diameter, 6 mm thickness) was used as point source excitation of the A_0 mode. The point transducer was bonded to the plate surface with Loctite 2-part epoxy glue. To ground the transducer, silver conductive paint was applied to the plate surface in a small region beneath the PZT disk transducer. The excitation signal was a 5-cycle sine wave modulated by a Hanning window at 75 kHz center frequency, generated using a programmable function generator (Agilent 33220 A, Agilent, Santa Clara, CA). The excitation signal was amplified to 75 V_{pp} (Krohn-Hite 7602 M wideband amplifier, Krohn-Hite, Brockton, MA) before being applied to the transducer. A laser vibrometer (Polytec OFV-505 sensor head, OFV-5000 vibrometer controller, Polytec, Waldbronn, Germany) was used to

measure the velocity of the out-of-plane displacement at the plate surface. The laser head was attached to a scanning rig, shown in Fig. 3(a), allowing for horizontal and vertical movement parallel to the specimen. Retroreflective tape was applied to the plate to improve the laser beam reflection and thus signal-to-noise ratio. Time signals were filtered using a 4th order Butterworth bandpass filter with cut-off frequencies of 50 and 100 kHz, respectively. The signals were recorded using a digital storage oscilloscope and averaged 20 times before being saved to a PC for further analysis in MATLAB. Radial lines, 100 mm length in 1 mm steps, were scanned at a distance 100 mm from the transducer as shown in Fig. 3(b). These measurements were used to calculate phase and group velocity for different wave propagation directions.

A line transducer shown in the inset of Fig. 4(a), consisting of a piezoceramic strip (PZT PIC-255, dimensions $40\text{ mm} \times 5\text{ mm} \times 1\text{ mm}$) and a steel backing mass ($40\text{ mm} \times 5\text{ mm} \times 5\text{ mm}$) was constructed. Aluminum conductive tape was applied to both faces of the PZT strip as electrodes [Fig. 4(b)]. The PZT strip and electrodes were then attached to the backing mass using double sided adhesive tape. Blu-tack was used as filling material at each end of the transducer to prevent short circuiting. The transducer was mounted on the rear side of the plate and pushed on the plate using a screw as shown in Fig. 4(a) to obtain repeatable clamping pressure. The outer face of transducer was wrapped in tape to protect the PZT strip as a thin layer of set honey was used to improve coupling, increasing signal amplitude. The line transducer was then rotated to achieve different wave propagation directions. To capture wave skew effects, lines of measurement points perpendicular to the wave launching direction (parallel to the line excitation) were scanned in 2 mm steps on the region covered with retroreflective tape. The lines were located 100, 125, 150, 175, and 200 mm from the line source.

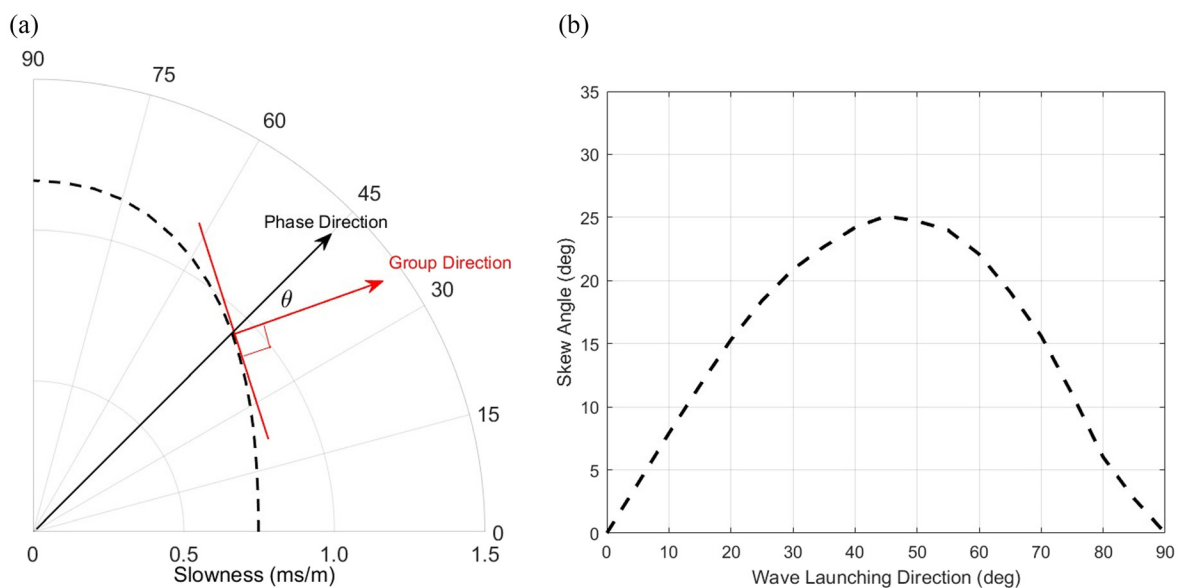


FIG. 2. (Color online) (a) Theoretical phase slowness curve for 3.6 mm thick CFRP at 75 kHz, calculated from dispersion curves. Phase and group directions denoted by arrows. (b) Variation in theoretical skew angle with phase direction.

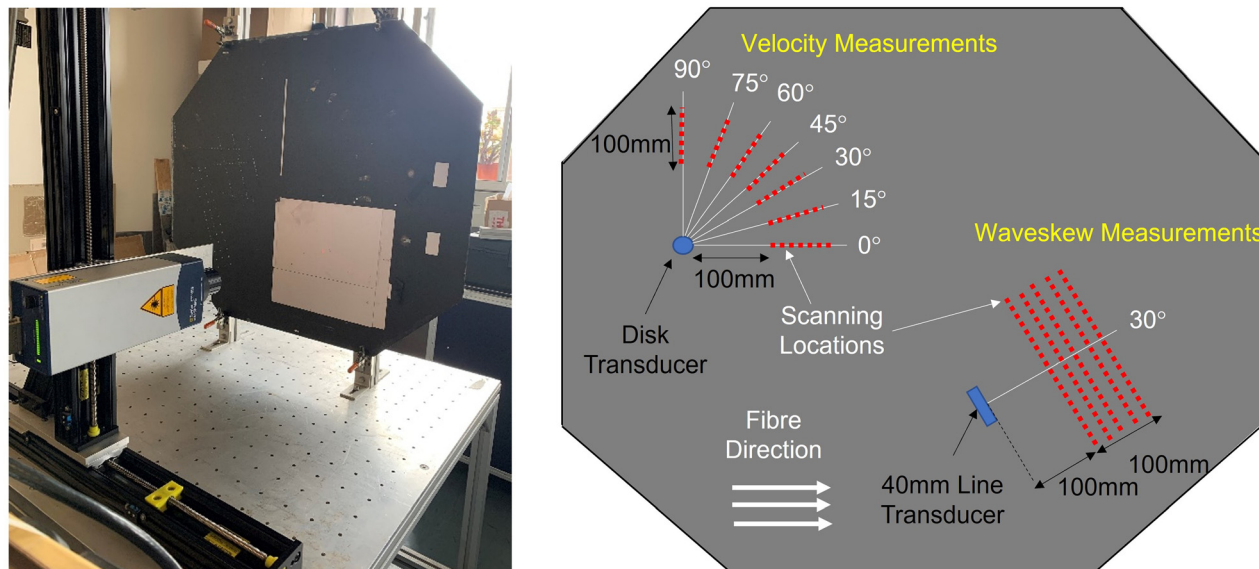


FIG. 3. (Color online) (a) Photograph of CFRP specimen and experimental setup. (b) Schematic of scanning patterns for velocity and wave skew measurements on CFRP specimen.

IV. RESULTS AND DISCUSSION

A. Directional dependence of velocity

The phase and group velocities of the A_0 mode were calculated for each wave launching direction and are shown in Fig. 5. To obtain the phase velocity, a fast Fourier transform (FFT) was performed on the time signals along a line of measurement points shown in Fig. 1(a). The phase angle at the center frequency of excitation ϕ was extracted for each measurement point and plotted against distance from the source, removing any 2π phase jumps. A linear fit was performed, and the gradient of the line extracted. The phase velocity was then calculated by multiplying the inverse of the gradient by a factor of $2\pi f$, where f is the center frequency of the excitation (75 kHz). Experiments using a widely employed PZT disk as an approximate point source do not fulfill the assumption of a plane wave front used to calculate theoretical dispersion curves. A correction must be performed on the raw velocity values to account for the anisotropic wave skew effect,³⁸ otherwise the phase velocities will be significantly underestimated (up to 12%) in wave launching directions with high skew angle. Employing the assumption from the theory that wave fronts stay parallel to the wave launching direction (phase direction), but their energy propagates in the group direction¹⁶ (given by the skew angle, see Fig. 2), the phase velocity must be calculated from the wave pulses in the group direction and then projected back in the phase direction [multiplication by factor $\cos(\theta_{\text{skew}})$] to match the theoretical assumption of a planar wave front.

To calculate the group velocity, the maximum amplitude of the signal was obtained from the Hilbert envelope. As the group velocity calculation is sensitive to pulse distortion due to dispersion, a narrowband bandpass 8th order Butterworth filter was applied to the time signals with cutoff frequencies 70 and 80 kHz, respectively. The arrival time of

the maximum amplitude was plotted against the distance from the source for each measurement point in a given direction. A linear fit was then performed, and the gradient

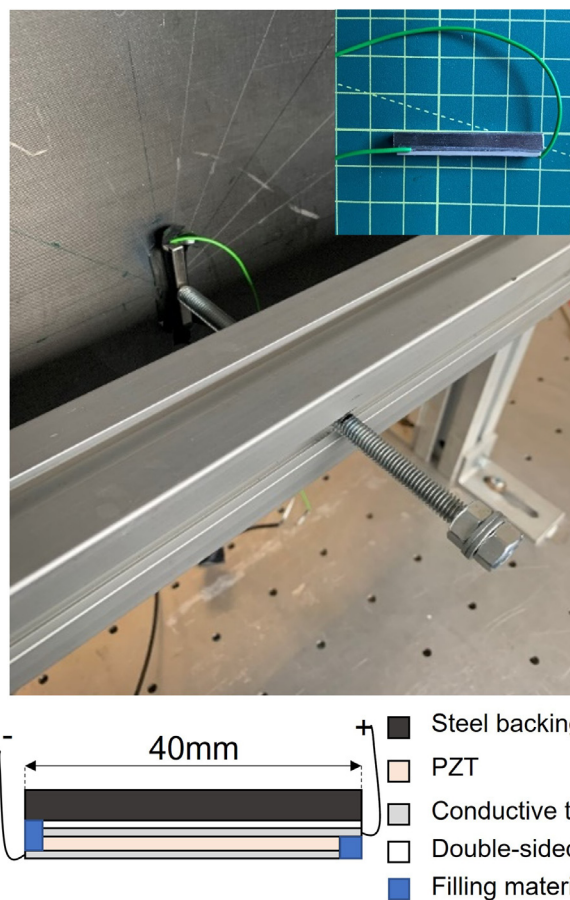


FIG. 4. (Color online) (a) Photograph of line transducer (inset) and clamping mechanism on rear of plate; (b) schematic of transducer construction.

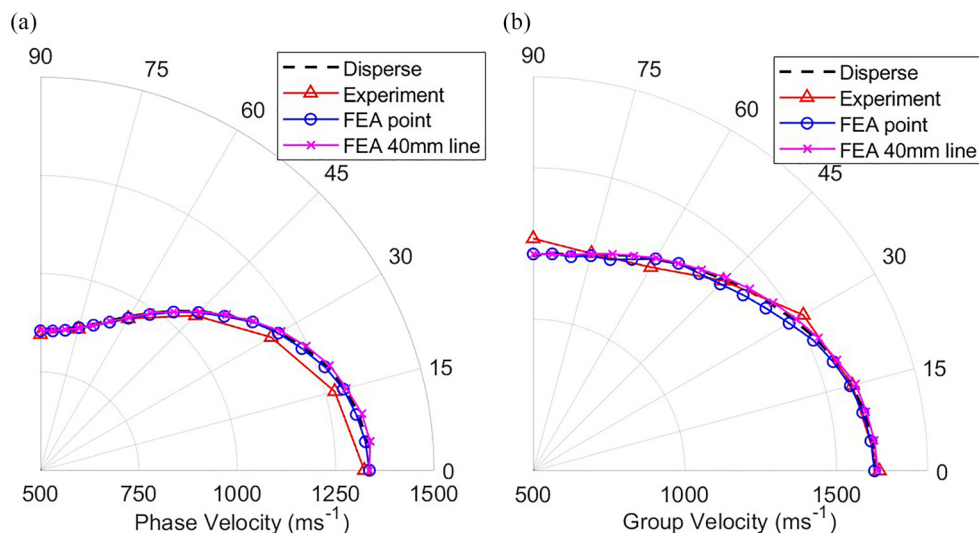


FIG. 5. (Color online) Measured, simulated, and theoretical (a) phase and (b) group velocity variation with propagation angle at 75 kHz center frequency.

of the line extracted. The group velocity is equal to the inverse of this gradient. The skew angle correction also needs to be applied to the group velocity to match theoretical assumptions.

Figure 5(a) shows measured and simulated phase velocity values at 75 kHz compared with the theoretical values obtained from Disperse. Very good agreement of the FEA evaluation for a line and point source with the theoretical values can be seen. The maximum difference is less than 1%, indicating that the correction for the wave skew due to anisotropy allows accurate determination of the phase velocity for a point source. Experimental results in general agree well and show the same angular dependence, but a maximum offset of 2% between theory and measurement can be observed in the 15° and 30° directions. This could be due to either experimental uncertainties or a slight offset in the assumed material properties. A similar trend can be observed for the group velocity values shown in Fig. 5(b). A small offset of up to 2% can be observed for the point source FEA results, with agreement within 1% along the principal axes. For the 40 mm line source, the corrected group velocity values show very good agreement within 1% of the theoretical values. The measured velocity values are in reasonable agreement with the FEA results.

These results indicate that care should be taken when measuring phase and group velocities in an anisotropic material, particularly if using a point source such as a PZT disk often selected for guided wave measurements. While the skew angle correction for a point source works well, some knowledge of the material anisotropy and expected wave skew angle is required. Overall, the FEA model has been demonstrated to accurately predict wave propagation behavior, showing good agreement with theory and experimental measurements.

B. Visualization of guided wave skew

In order to understand the influence of material anisotropy on wave propagation, the wave steering behavior in the

plate should be determined. The images in Figs. 6 and 7 visualize the time traces obtained along each line of measurement points, equivalent to a B-scan. Figure 6 shows the simulated out-of-plane displacement time traces from a 40 mm line source at each measurement point for lines of points located 100, 150, 200 mm from the source in the 0°, 30°, 60°, and 90° wave launching directions. In the 0° direction (top row, Fig. 6) the wave pulse does not deviate from the initial propagation direction and does not show significant widening as it propagates along the plate. In the 30° direction (2nd row, Fig. 6) significant deviation from the wave launching direction towards the 0° direction can be observed, in addition to slight widening of the beam. In the 60° direction, the beam is skewed towards the 0° direction to a similar degree as the 30° direction; however, the beam widening at 60° is much more significant. In the 90° direction no beam steering is observed, but significant beam widening occurs as the wave pulse propagates. This is partly due to the energy focusing along the fibers, perpendicular to the propagation direction. In each of the wave launching directions the orientation of the wavefronts remains parallel to the wave propagation direction, irrespective of the degree of steering experienced, as expected.

Figure 7 shows the measured out-of-plane displacement time traces (B-scan equivalent) at 100, 150, and 200 mm from the 40 mm line transducer in the 0°, 30°, 60°, and 90° directions. As expected, the measured wave pulse is less uniform than for the simulations, however the wave steering and spreading behavior is similar. In the 0° direction, the main wave pulse remains focused along the wave launching direction with limited beam spreading. In the 30° direction the wave pulse consists of two regions of high amplitude, which is not observed in the FEA. Significant wave steering from the initial direction can be observed, consistent with the FEA predictions. Some beam spreading can be observed, particularly at 200 mm, where the gap between the two wave pulses has significantly increased. In the 60° direction,

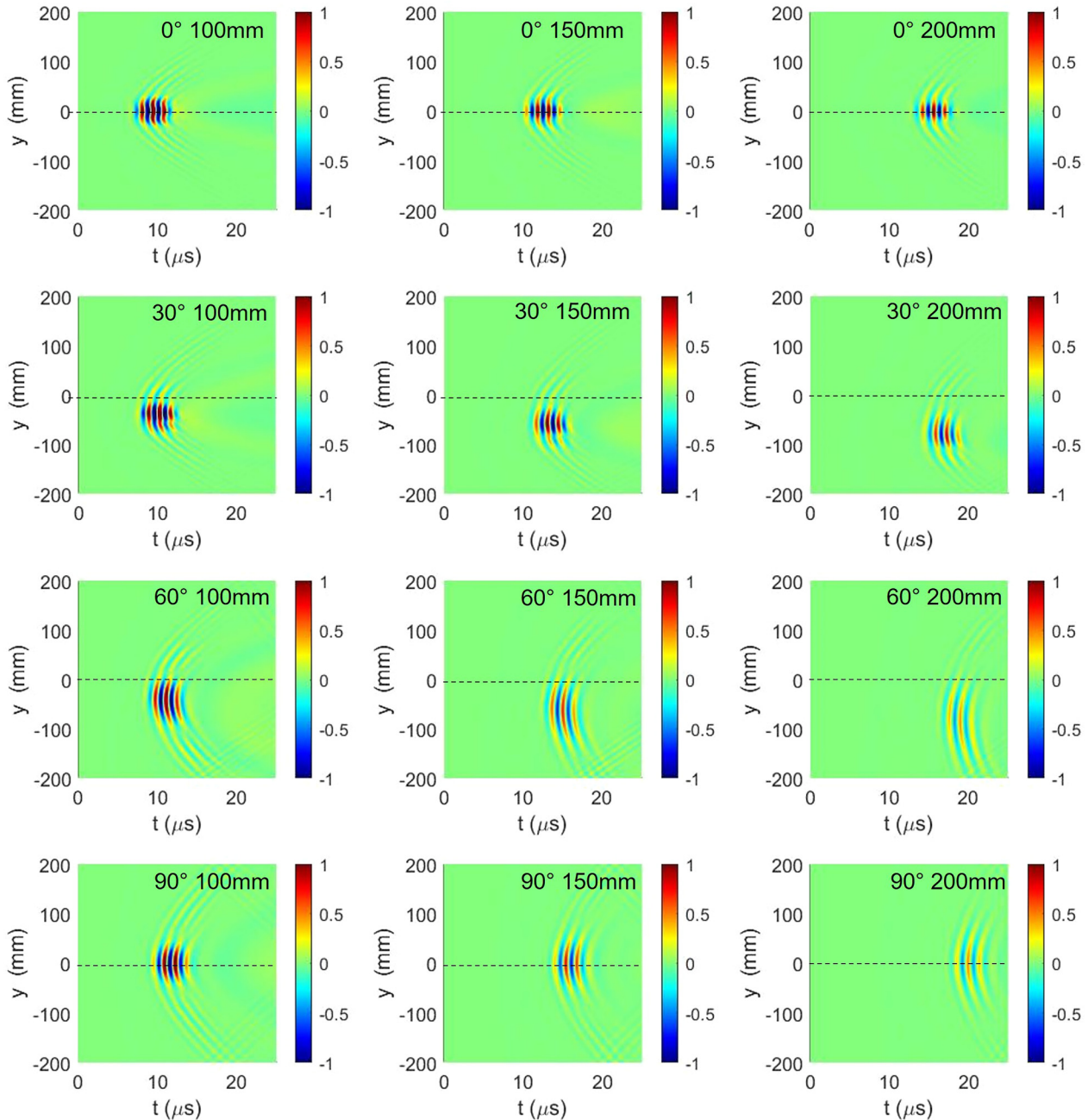


FIG. 6. (Color online) Normalized displacement time traces along a single line of measurement points (parallel to the excitation line source) for A_0 mode obtained from FEA (the equivalent of a B-scan). Wave launching angles of 0° , 30° , 60° , and 90° at three lines of measurement points located 100, 150, and 200 mm from the excitation location, respectively. The wave launching direction is represented by a dashed line at $y = 0$ mm.

the main central pulse shows wave skewing behavior as expected. The central pulse, originating from the front of the line source, is more difficult to distinguish in this direction, particularly at 100 mm from the source, but also displays beam spreading. No steering is observed in the 90° direction as expected, but spreading of the central pulse occurs. The measurements show that beam spreading increases with wave launching angle. As seen from the FEA results, the wavefronts remain oriented parallel to their initial launching direction. In the experimental measurements the amplitude of guided waves decays more severely as the propagation angle is increased, compared to the FEA.

In order to analyze the energy distribution of the line wave excitation in more detail, the maximum amplitude of the wave pulse was calculated at each measurement point along the five parallel lines of measurement points. Figures 8(a) and 8(b) show the simulated and measured amplitudes for the A_0 mode propagating along the 0° wave launching direction. The measurement lines at 125 and 175 mm from the source have been omitted for clarity. No wave skew is observed for simulated results [Fig. 8(a)] as the peaks are aligned. No beam spreading is visible due to energy focusing effects. The main peak of the experimentally measured wave pulse also shows no wave skewing and limited beam

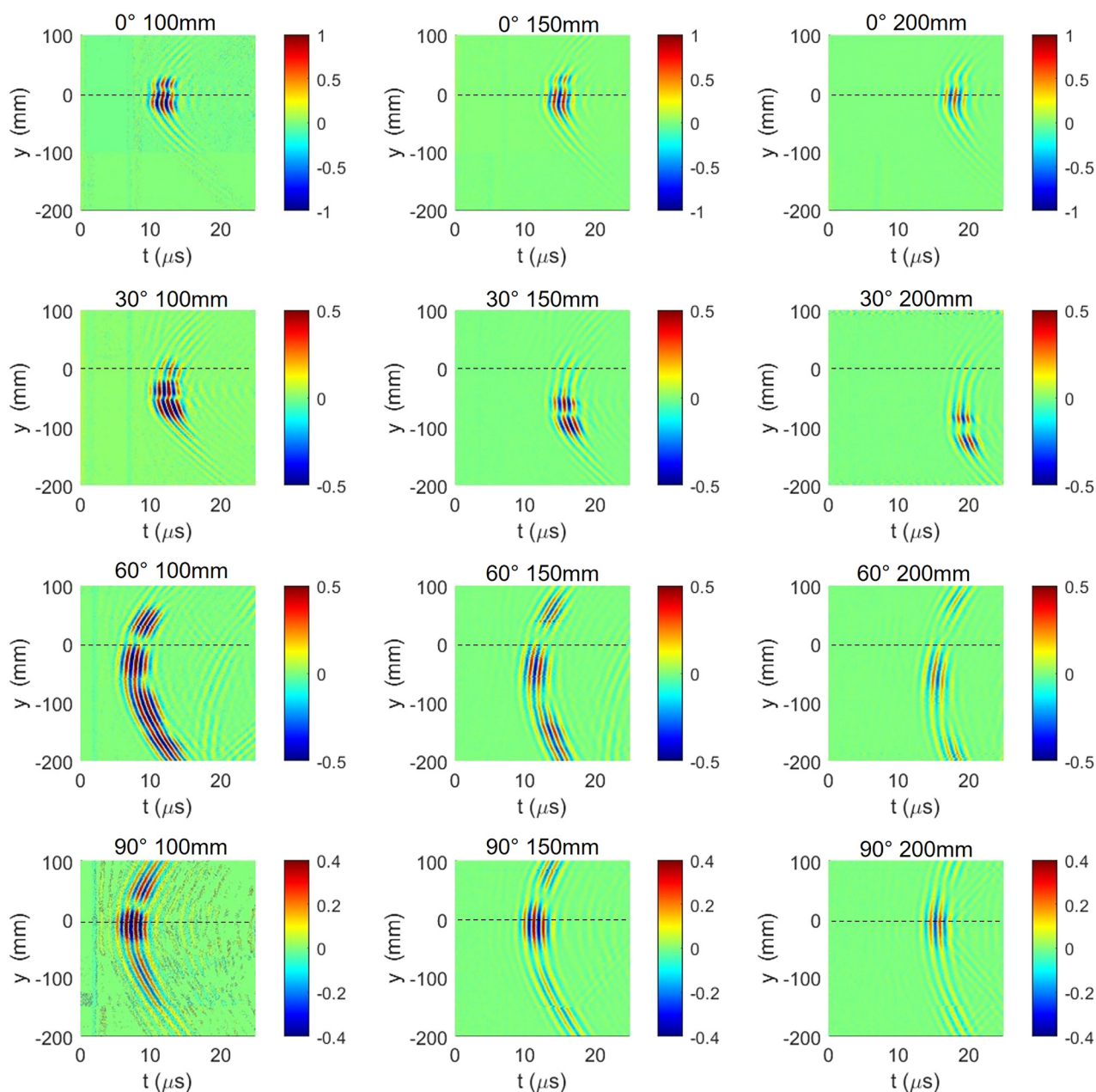


FIG. 7. (Color online) Experimentally measured displacement time traces along a single line of measurement points (parallel to excitation line source, equivalent to B-scan) for A_0 mode generated by line transducer (40 mm length). Wave launching angles of 0° , 30° , 60° , and 90° at three lines of measurement points located 100, 150, and 200 mm from excitation location, respectively. The wave launching direction is represented by a dashed line at $y = 0$ mm.

spread [Fig. 8(b)]. The second peak to the right of the main peak is caused by nonuniformity in the experimental line excitation and is due to waves being generated from the ends of the transducer. Figures 8(c) and 8(d) show the simulated and measured amplitudes along the 90° wave launching direction. In both measurement and simulation no wave skew is observed as the peaks are aligned, but significant beam widening, consistent with the images in Figs. 6 and 7, can be observed.

The measured and simulated amplitudes along the 30° and 60° wave launching directions are presented in Figs. 9(a) and 9(b) and Figs. 9(c) and 9(d), respectively. Wave skewing can be observed as the main amplitude peaks shift

to the left with increasing distance from the source. In the 30° direction some beam spreading is observed in the FEA, but this is more difficult to observe in the experiments due to the double amplitude peak present. The double peak is not present in the FEA initially, although as the wave pulse propagates, a secondary peak starts to develop to the right of the main pulse. The double peak in the experiments is likely due to the imperfect line excitation, but in this case, could be caused by destructive interference at the center of the transducer (length approximately twice wavelength at 75 kHz). For the 60° wave launching direction beam skewing again is observed in both the experiment and simulation. Beam spreading in the 60° direction is more severe than in

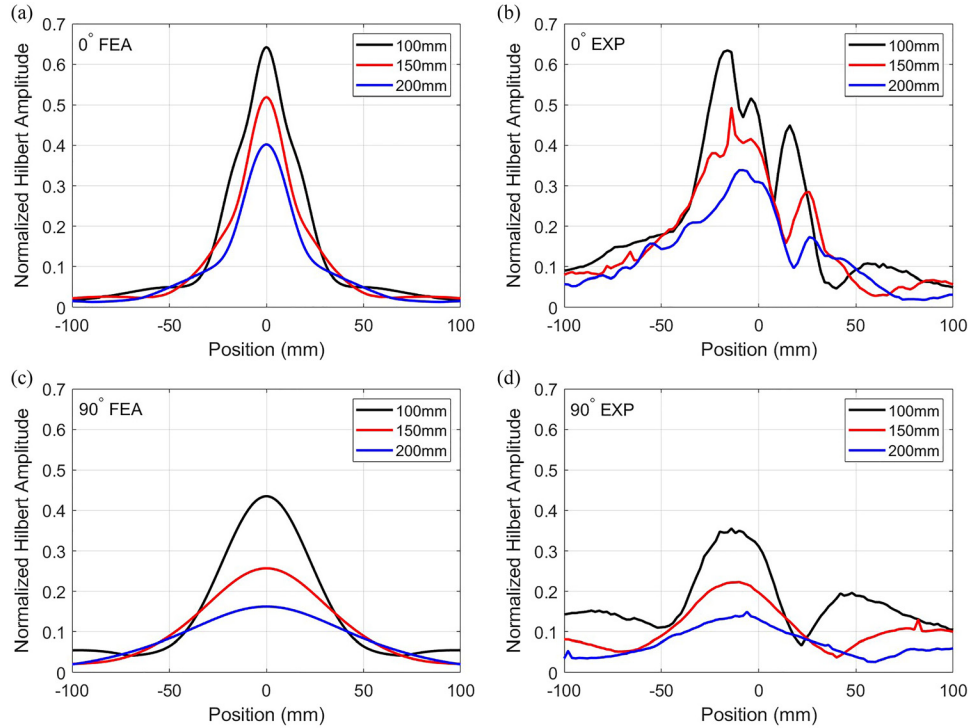


FIG. 8. (Color online) Normalized maximum wave pulse envelope (Hilbert transform) amplitude along lines of measurement points located 100, 150, and 200 mm from line source for (a) 0° direction FEA; (b) 0° direction experiment; (c) 90° direction FEA; (d) 90° direction experiment.

the 30° direction as expected, however, slightly counterintuitively, appears to also be greater than the spreading observed in the 90° direction.

C. Calculation of guided wave skew angles and beam spreading

The previous results have shown that the position of the wave pulse changes with propagation direction in the non-principal directions, where there is a non-zero skew angle. One method to estimate the position of the wave pulse is to simply take the location of the maximum amplitude of the wave pulse at each location.⁴³ However, this procedure becomes inaccurate when the excitation consists of multiple peaks, e.g., as shown in Fig. 9(b). In order to estimate the position of the wave pulse the weighted sum of three standard Gaussian functions was fitted to each amplitude curve,

$$f(x) = a_1 \exp \left[-\left(\frac{x - b_1}{c_1} \right)^2 \right] + a_2 \exp \left[-\left(\frac{x - b_2}{c_2} \right)^2 \right] + a_3 \exp \left[-\left(\frac{x - b_3}{c_3} \right)^2 \right], \tag{3}$$

where the coefficients a_n represent the amplitude of each Gaussian peak, the coefficients b_n represent the centroid of each peak, and coefficients c_n are related to the width of each peak. To estimate the true center of the wave pulse, a weighted average of the peak centroids was performed (i.e., b_n weighted with respect to a_n). Several types of fitting functions were investigated including Gaussian and Lorentzian

functions and the sum of multiple Gaussian functions. For smooth amplitude curves [e.g., Fig. 8(a)] a single Gaussian already provided a good fit. However, the weighted sum of three Gaussian functions, as given in Eq. (3), provided the best fit ($R^2 > 0.99$) for all cases, as shown in Fig. 10 for the FEA [Fig. 10(a)] and experimental [Fig. 10(b)] results, as it was able to match the multiple peaks.

The fitting procedure was performed on both the simulated and experimental curves for each wave launching direction. The skew angles were calculated by plotting the averaged center location of each amplitude curve against distance from the source. A linear fit was then performed, and the wave skew angle was calculated from the inverse tangent of the line gradient. Skew angles from the fitted curves were compared with the theoretical values obtained from the phase slowness curve [Fig. 11(a)]. In the principal directions, zero skew angle is observed as expected. The maximum skew angle of 28.3° is measured for the 45° wave launching direction with almost symmetric skew angles either side of this. The skew angles are slightly higher for the 0°–45° directions than for the 45°–90° directions, likely due to the effect of energy focusing causing greater beam steering in these directions. Overall, there is good agreement between theory and FEA. However, the experimentally measured skew angles are slightly higher than expected in the high skew directions (from 30° to 60°). As the experimentally measured point source velocities showed good agreement with theory, the experimental error in the wave skew angles could likely be caused by the quality of the line source excitation leading to a more complicated amplitude pattern. The measured skew angles follow the overall

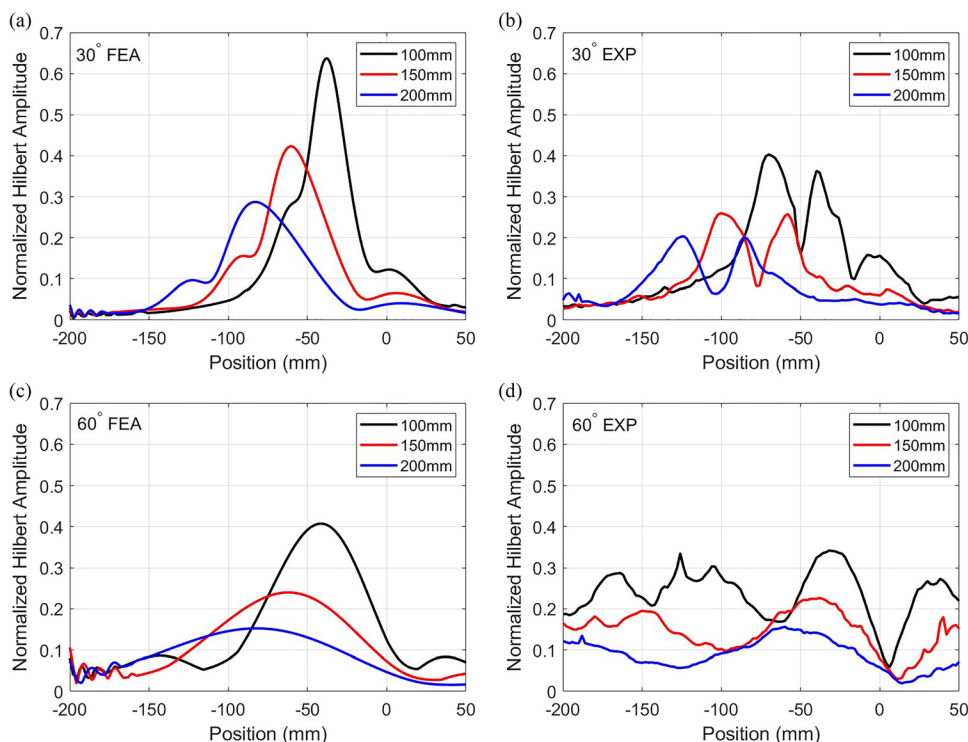


FIG. 9. (Color online) Normalized wave pulse envelope (Hilbert transform) amplitude along lines of measurement points located 100, 150, and 200 mm from line source for (a) 30° direction FEA; (b) 30° direction experiment; (c) 60° direction FEA; (d) 60° direction experiment.

pattern of the theoretical values and agree well with theory in the directions with lower skew angles. These results show that severe skew angles can occur in this unidirectional CFRP specimen, which could impact guided wave SHM. High skew angles could lead to errors in locating damage, as the beam is steered away from the wave launching direction, potentially leading to regions where guided waves do not propagate due to the severe steering.

To estimate the beam spreading, the full width at half maximum (FWHM) of the wave pulse was tracked over distance. The FWHM of a three term Gaussian function can be calculated as

$$FWHM = 2c_{av}\sqrt{2\ln 2}. \tag{4}$$

Here, c_{av} is the average of the c_n coefficients in Eq. (3) weighted with respect to the corresponding amplitude coefficients a_n . The FWHM was calculated for each of the five amplitude curves (shown for 30° wave launching direction in Fig. 10), plotted against distance from the source, and a linear fit was performed. The gradient was extracted from the fit and the beam spreading angle was estimated by taking the inverse tangent of this gradient.

The measured and simulated beam spread angles were calculated for each wave launching direction and are shown

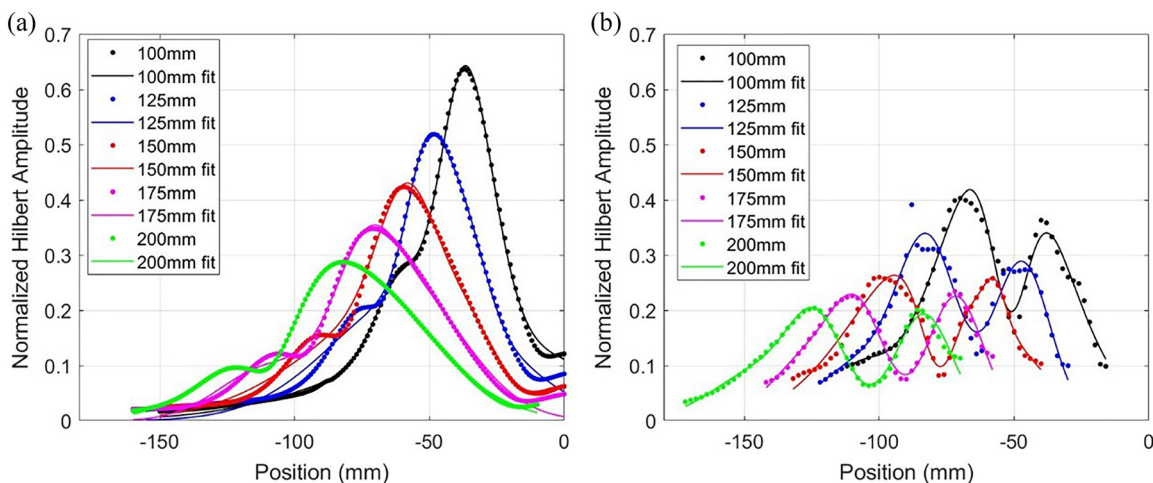


FIG. 10. (Color online) Normalized maximum Hilbert amplitude for 30° wave launching direction with triple Gaussian curve fitting for (a) FEA and (b) experiment.

in Fig. 11(b). The theoretical anisotropy factor A [Eq. (2)] was calculated for each of the wave launching directions and is also plotted. The additional factor of $(\cos(\theta_{skew}))^{-2}$ in A compared to the divergence D [Eq. (1)] gave a slightly better match to the FEA and experimental results. It should be noted that the anisotropy factor is a dimensionless quantity and thus cannot directly be compared to the calculated beam spread angle. However, the overall physical behavior described by the anisotropy coefficient is similar. For example, A reaches a maximum in the 75° wave launching direction. This indicates that the beam will be widening most rapidly at 75° ($A > 1$), matching the measured maximum beam spread angles calculated from the FEA and experimental evaluation. The anisotropy factor is dependent on the curvature of the slowness curve and so accurate knowledge of the variation of phase velocities with propagation direction in anisotropic materials is required. It should be noted that the Maris factor, which can be used to predict energy focusing,³⁹ is distinct from the anisotropy factor, but also related to the curvature of the slowness curve.

Low beam spreading is observed for the FEA results at 0° and 15° , as there is a large degree of energy focusing along the fiber direction at these wave launching angles. The spreading angle then steadily increases as the wave launching direction diverts from the fiber orientation. The highest beam spreading, slightly counterintuitively, is observed at 75° . This is likely due to a combination of energy focusing along the almost perpendicular fiber directions stretching the beam, as seen in the 90° direction, in addition to wave skewing effects enhancing the degree of spreading. Severe beam spreading, as observed in Fig. 11(b), could lead to significantly lower detected signal amplitudes in certain directions, indicating regions where damage could be difficult to detect. The measured beam spread angles generally follow a similar pattern to the FEA results; however, the FEA predicts slightly higher beam spreading for most propagation directions. The accuracy of the experimentally

measured beam spread angles is limited by the quality of the line excitation, which did not match the assumed uniform amplitude distribution. It should be noted that the anisotropic wave propagation effects in a unidirectional laminate will be larger than that of a cross-ply or quasi-isotropic CFRP layup. The beam steering and spreading behavior in these laminates will be smaller but could be significant enough to reduce the accuracy of guided wave based SHM.

V. CONCLUSIONS

Anisotropic guided wave propagation effects were investigated for the A_0 mode in a unidirectional CFRP laminate. The directional dependence of phase and group velocity from a point and a 40 mm line source was investigated through experimental measurements and finite element modelling. Good agreement between measurements, FEA, and theoretical velocity values was observed, provided that a velocity correction is applied to incorporate anisotropic wave skewing effects. Numerical and experimental studies of the wave skewing behavior in multiple incident wave directions were performed. Zero skew angle was observed in the principal (0° , 90° relative to fiber orientation) directions with maximum skewing occurring at 45° for the experimental, FEA, and theoretical analysis. The skew angles calculated from the FEA showed good agreement with theoretical values calculated from the phase slowness curve. The measured skew angles were slightly higher than predicted in directions with the largest degree of skewing (30° , 45° , 60°). Beam spreading was estimated from the experimental and simulation results. Limited spreading occurs in the 0° and 15° directions due to energy focusing along the fibers occurring in these directions, leading to higher observed amplitudes. As the wave launching direction moves away from the fiber directions, the beam spreading increases significantly. The beam spreading angle was compared with the anisotropy factor, calculated from the theoretical slowness curve. While a direct

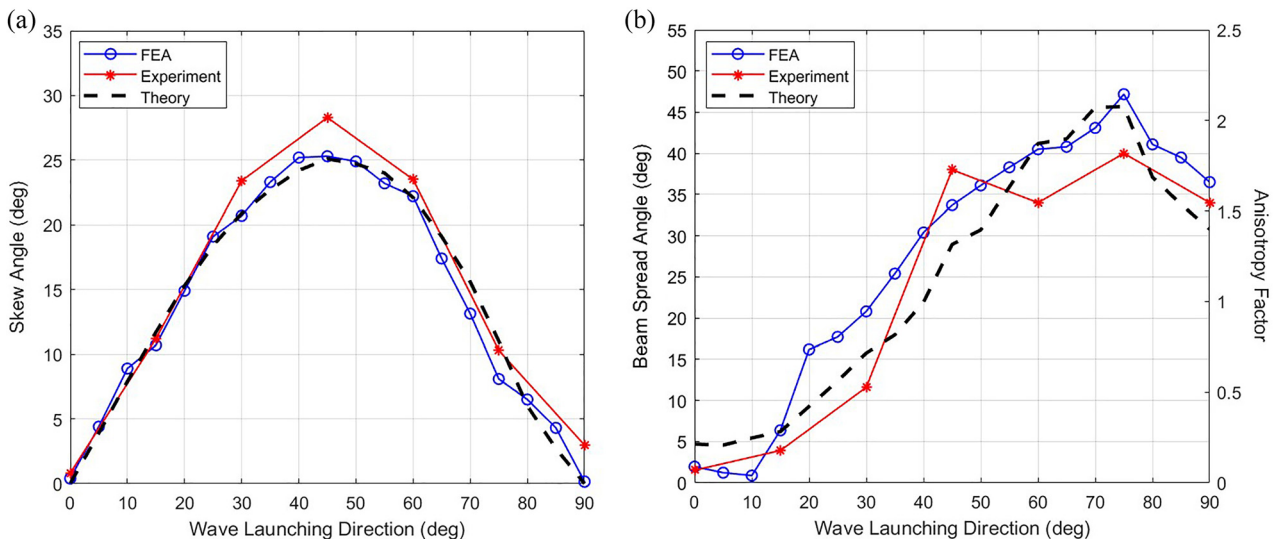


FIG. 11. (Color online) (a) Measured, simulated, and theoretical skew angles for wave launching directions between 0° and 90° ; (b) estimated beam spread angle with wave launching direction from FEA and experimental measurement, overlaid with anisotropy factor.

comparison cannot be made, the physical behavior observed in the experiments and simulations matched the theoretical prediction. Guided waves propagating in unidirectional composite laminates, such as the specimen used for this study, will experience greater anisotropic effects than in other layups. However, the effects studied here will also occur to some degree in specimens with cross-ply and quasi-isotropic layups. Anisotropic effects such as severe skew angles and beam spreading, as observed for this specimen, could lead to reduced accuracy in damage location or regions where little to no guided wave amplitude can propagate in composite plates. Therefore, anisotropic effects should be considered when designing guided wave SHM systems.

¹W. J. Cantwell and J. Morton, "Geometrical effects in the low velocity impact response of CFRP," *Compos. Struct.* **12**, 39–59 (1989).
²K. Diamanti, J. M. Hodgkinson, and C. Soutis, "Detection of low-velocity impact damage in composite plates using lamb waves," *Struct. Health Monit.* **3**, 33–41 (2004).
³T. W. Shyr and Y. H. Pan, "Impact resistance and damage characteristics of composite laminates," *Compos. Struct.* **62**, 193–203 (2003).
⁴O. Putkis, R. P. Dalton, and A. J. Croxford, "The anisotropic propagation of ultrasonic guided waves in composite materials and implications for practical applications," *Ultrasonics* **65**, 390–399 (2016).
⁵M. J. S. Lowe, G. Neau, and M. Deschamps, "Properties of guided waves in composite plates, and implications for NDE," *AIP Conf. Proc.* **700**, 214–221 (2004).
⁶J. S. Hall, P. Fromme, and J. E. Michaels, "Guided wave damage characterization via minimum variance imaging with a distributed array of ultrasonic sensors," *J. Nondestruct. Eval.* **33**, 299–308 (2014).
⁷P. Wilcox, M. Lowe, and P. Cawley, "Effect of dispersion on long-range inspection using ultrasonic guided waves," *NDT&E Int.* **34**, 1–9 (2001).
⁸K. J. Schubert and A. S. Hermann, "On attenuation and measurement of Lamb waves in viscoelastic composites," *Compos. Struct.* **94**, 177–185 (2011).
⁹H. Mei, M. F. Haider, R. James, and V. Giurgiutiu, "Pure S0 and SH0 detections of various damage types in aerospace composites," *Compos. B Eng.* **189**, 107906 (2020).
¹⁰K. Hayat and S. K. Ha, "Low-velocity impact-induced delamination detection by use of the S0 guided wave mode in cross-ply composite plates: A numerical study," *J. Mech. Sci. Technol.* **28**, 445–455 (2014).
¹¹S. Gupta and P. Rajagopal, "Effect of ply orientation and through-thickness position of delamination on the reflection of fundamental symmetric S0 Lamb mode in GFRP composite plate structures," *Ultrasonics* **90**, 109–119 (2018).
¹²N. Guo and P. Cawley, "The interaction of Lamb waves with delaminations in composite laminates," *J. Acoust. Soc. Am.* **94**, 2240–2246 (1993).
¹³A. Bernard, M. J. S. Lowe, and M. Deschamps, "Guided waves energy velocity in absorbing and non-absorbing plates," *J. Acoust. Soc. Am.* **110**, 186–196 (2001).
¹⁴F. Hervin and P. Fromme, "Anisotropy influence on guided wave scattering for composite structure monitoring," *Struct. Health Monit.* (published online 2022).
¹⁵G. Neau, M. J. S. Lowe, and M. Deschamps, "Propagation of Lamb waves in anisotropic and absorbing plates: Theoretical derivation and experiments," *AIP Conf. Proc.* **615**, 1062–1069 (2002).
¹⁶E. Glushkov, N. Glushkova, A. Eremin, and R. Lammering, "Group velocity of cylindrical guided waves in anisotropic laminate composites," *J. Acoust. Soc. Am.* **135**, 148–154 (2014).
¹⁷J. L. Rose, *Ultrasonic Guided Waves in Solid Media* (Cambridge University Press, Cambridge, UK, 2014).
¹⁸H. Gao, "Ultrasonic guided wave mechanics for composite material structural health monitoring," Ph.D. thesis, The Pennsylvania State University, College Park, PA (2007).
¹⁹P. Fromme, M. Pizzolato, J. Robyr, and B. Masserey, "Lamb wave propagation in monocrystalline silicon wafers," *J. Acoust. Soc. Am.* **143**, 287–295 (2018).

²⁰L. Yu and Z. Tian, "Guided wave phased array beamforming and imaging in composite plates," *Ultrasonics* **68**, 43–53 (2016).
²¹F. Yan and J. L. Rose, "Time delay comb transducers for aircraft inspection," *Aeronaut. J.* **113**, 417–427 (2009).
²²F. Yan and J. L. Rose, "Guided wave phased array beam steering in composite plates," *Proc. SPIE* **6532**, 65320G (2007).
²³W. K. Chiu, L. R. F. Rose, and N. Nadarajah, "Scattering of the fundamental anti-symmetric Lamb wave by a mid-plane edge delamination in a fiber-composite laminate," *Procedia Eng.* **188**, 317–324 (2017).
²⁴W. B. Williams, T. E. Michaels, and J. E. Michaels, "Estimation and application of 2-D scattering matrices for sparse array imaging of simulated damage in composite panels," *AIP Conf. Proc.* **1806**, 020014 (2017).
²⁵J. A. Ogilvy, "Ultrasonic beam profiles and beam propagation in an austenitic weld using a theoretical ray tracing model," *Ultrasonics* **24**, 337–347 (1986).
²⁶B. P. Newberry and R. B. Thompson, "A paraxial theory for the propagation of ultrasonic beams in anisotropic solids," *J. Acoust. Soc. Am.* **85**, 2290–2300 (1989).
²⁷H. J. Maris, "Effect of finite phonon wavelength on phonon focusing," *Phys. Rev. B* **28**, 7033–7037 (1983).
²⁸V. I. Balakshy and S. N. Mantsevich, "Propagation of acoustic beams in a paratellurite crystal," *Acoust. Phys.* **58**, 549–557 (2012).
²⁹S. N. Mantsevich, "Thallium bromide iodide crystal acoustic anisotropy examination," *Ultrasonics* **75**, 91–97 (2017).
³⁰B. Chapuis, N. Terrien, and D. Royer, "Excitation and focusing of Lamb waves in a multilayered anisotropic plate," *J. Acoust. Soc. Am.* **127**, 198–203 (2010).
³¹C. Potel, S. Baly, J. de Belleval, M. Lowe, and P. Gagnon, "Deviation of a monochromatic Lamb wave beam in anisotropic multilayered media: Asymptotic analysis, numerical and experimental results," *IEEE Trans. Ultrason. Ferroelectr. Freq. Control* **52**, 987–1001 (2005).
³²D. Chronopoulos, "Wave steering effects in anisotropic composite structures: Direct calculation of the energy skew angle through a finite element scheme," *Ultrasonics* **73**, 43–48 (2017).
³³C. Hakoda and C. J. Lissenden, "Application of a general expression for the group velocity vector of elastodynamic guided waves," *J. Sound Vib.* **469**, 115165 (2020).
³⁴H. Cho, S. Choi, and C. J. Lissenden, "Effect of skew angle on second harmonic guided wave measurement in composite plates," *AIP Conf. Proc.* **1806** 060002 (2017).
³⁵G. Neau, M. Deschamps, and M. J. S. Lowe, "Group velocity of Lamb waves in anisotropic plates: Comparison between theory and experiments," *AIP Conf. Proc.* **557**, 81–88 (2001).
³⁶L. Wang and F. G. Yuan, "Group velocity and characteristic wave curves of Lamb waves in composites: Modeling and experiments," *Compos. Sci. Technol.* **67**, 1370–1384 (2007).
³⁷A. De Luca, D. Perfetto, A. Pulverino, A. Aversano, and F. Caputo, "Finite element modeling approaches, experimentally assessed, for the simulation of guided wave propagation in composites," *Sustainability* **14**, 6924 (2022).
³⁸J. Zhao, J. Qiu, and H. Ji, "Reconstruction of the nine stiffness coefficients of composites using a laser generation based imaging method," *Compos. Sci. Technol.* **126**, 27–34 (2016).
³⁹B. Chapuis, N. Terrien, and D. Royer, "Modeling and experimental investigations of Lamb waves focusing in anisotropic plates," *J. Phys. Conf. Ser.* **269**, 012020 (2011).
⁴⁰K. I. Salas and C. E. S. Cesnik, "Guided wave structural health monitoring using CLoVER transducers in composite materials," *Smart Mater. Struct.* **19**, 015014 (2010).
⁴¹F. Ihlenburg, *Finite Element Analysis of Acoustic Scattering* (Springer, New York, 1998).
⁴²B. Pavlakovic, M. Lowe, D. Alleyne, and P. Cawley, "Disperse: A general purpose program for creating dispersion curves," *Rev. Prog. Quant. Nondestruct. Eval.* **16**, 185–187 (1997).
⁴³F. Hervin and P. Fromme, "Anisotropy influence on guided wave propagation and steering in unidirectional CFRP," in *Proceedings of the 49th Annual Review of Progress in Quantitative Nondestructive Evaluation*, San Diego, CA (July 25–27, 2022), V001T03A007. ASME.